Journal of Fluids and Structures (1999) **13,** 791–811
Article No.: jfls. 1999.0249, available online at http://www. idealibrary.com on IDEAL®

VORTEX SHEDDING OF BLUFF BODIES: A REVIEW

M. MATSUMOTO

Department of Global Environment Engineering, Kyoto University, Yoshida Honmachi, Sakyo-ku 6068501, Japan

(Received 21 November 1998 and in revised form 15 June 1999)

In this paper the various types of vortex generation and the related response characteristics of bluff bodies are described. The vortices are, in general, generated by a certain stimulation, leading to one- or two-shear layer instability; the related unsteady forces could excite flexible structures such as tall towers, tall buildings and long-span bridges. Karman vortex shedding is well known as the alternate shedding vortex behind bluff bodies, but the one-shear layer instability related vortices and symmetrical vortex shedding should also be taken into account as additional mechanisms for the evaluation of structural safety, because they result in structural response at comparatively low wind speeds. In this paper, the symmetrical vortex shedding, which is enhanced by the longitudinally fluctuating flow for 2-D rectangular cylinders with a 0.5 side ratio, and one-shear layer related vortices, which are generated on the side surfaces of flat 2-D rectangular cylinders and many bridge girder box sections by the stimulation of body motion or applied sound, are introduced. Furthermore, as a peculiar 3-D vortex, the "axial vortex", which is formed in near wake of inclined cables and then over restricted velocity ranges, is also discussed.

1. INTRODUCTION

VORTEX-INDUCED VIBRATION is one of the major issues concerning flexible structures subjected to cross-flow, such as long-span bridges, tall buildings, tall towers, and so on. To be able to find the appropriate countermeasure to suppress the aerodynamic response, the generation mechanism of this response should be clarified first. However, because of the complex geometrical shapes of actual structures, the flow patterns around them and their related response is also complex; therefore, the fluid–structure interaction has been investigated for simplified structural sections only, such as 2-D rectangular cylinders, H-shaped cylinders, circular cylinders and so on, and mainly in smooth flows. The vortices could be classified as follows: two-shear-layer related vortices (including the Karman vortex streets and symmetrical vortices), one-shear-layer related vortices, 3-D vortices (including the tip vortex and axial vortex), and others.

Bearman & Trueman (1972) and Mizota & Okajima (1981) discussed the drag force related to the formation position of the Karman vortices behind 2-D rectangular cylinders with various side ratios, and they concluded that the close formation of the rectangular rear faces make the drag force large; they also explained the Nakaguchi peak (Nakaguchi *et al.* 1968) of the drag force of a 2-D rectangular cylinder with the specific side ratio of 0·64. King (1977) showed the existence of symmetrical vortex shedding behind a circular cylinder at the reciprocal reduced velocity of one-fourth of the Karman vortex resonance reduced velocity, where in-line vibration could be excited. Knisely *et al.* (1986) also visualized a similar symmetrical vortex shedding behind a 2-D rectangular cylinder with a side ratio of 0·5 in a longitudinally harmonically fluctuating flow in a water flume. Williamson (1986) reported

0889–9746/99/100791 + 21 $30.00

complicated forms of Karman vortex shedding, such as oblique shedding, and also 3-D characteristics around 2-D circular cylinders at a quite low Reynolds numbers.

Furthermore, Shimada & Meng (1998), by means of advanced CFD analysis, pointed out that Karman vortex shedding tends to be quite weak or vanishing at the critical side ratios of 2·8 and 6·0 for 2-D rectangular cylinders, where the Strouhal number suddenly changes with varying side ratio. Matsumoto *et al.* (1988) reported that the Strouhal number associated with Karman vortex-shedding is dependent on the angle of attack, which modifies the flow pattern around the body, for 2-D rectangular cylinders with a side ratio of 2·0.

On the one-shear-layer related vortex generation, Parker & Welsh (1983), Rockwell & Knisely (1978), Komatsu & Kobayashi (1980), Nakamura & Nakashima (1986) and Shiraishi & Matsumoto (1983) discussed the vortex formation characteristics based on wind tunnel or the water flume tests. On the other hand, for cylindrical flexible towers or for an inclined cable of cable-stayed bridges, the velocity-restricted vibration appears at higher reduced velocity than Karman vortex-shedding resonance reduced velocity. A vortex from the free end of a tower is called as "tip vortex" by Kitagawa *et al.* (1997), and a vortex in the near wake of an inclined cable is called an "axial vortex" by Matsumoto (1998). In this paper, the recent topics on vortex generation and the vortex-related excitation of structures are introduced and discussed.

2. THE VORTEX-SHEDDING EXCITATION OF RECTANGULAR CYLINDERS AND BRIDGE GIRDERS

Flow visualization around simplified bridge box girders and plate girders, which are flat rectangular cylinders, flat H-shaped ones, flat hexagonal ones, flat trapezoidal cylinders, and so on, under forced heaving or torsional motion in a water flume, showed both vortex generation and vortex convection along the body side-surface towards the trailing edge. A secondary vortex was also found in the near wake at the trailing edge, induced by body motion [see Figures 1(a) and 1(b), which are for 2-D rectangular cylinders with $B/D = 8{\cdot}2$ and $B/D = 2$, respectively, under heaving motion]. From the film of the visualized flow pattern, taken by a high-speed motion camera and from the direct measurement of the unsteady pressure distribution on the body side surface, the average convection velocity of this vortex from the leading edge of the body to the trailing edge, has been measured to be approximately 60% of the approach flow velocity.

For heaving motion, the vortex generated at the leading edge reaches the trailing edge, where it coalesces with the trailing edge secondary vortex and an intensive vortex can, in consequence, be shed in one cycle motion at the particular reduced velocity where the vortex-induced vibration appears; this was called "low-speed vortex excitation" by Nakamura & Nakashima (1986). Besides, this coalescence of two vortices, in a heaving motion at a related specified reduced velocity, can occur after two cycles, three cycles or more of heaving motion. This coalescence condition is formulated as follows (Shiraishi & Matsumoto 1983):

$$0{\cdot}6nVT_0 = B, \tag{1}$$

after n cycles of heaving motion ($n = 1, 2, 3, \ldots$), where V is the oncoming flow velocity, T_0 the natural period of heaving motion, and B the body chord-length in the longitudinal direction. The following critical onset reduced velocity for heaving vortex shedding vibration is obtained from equation (1):

$$V_{\mathrm{rcr}} = (1/0{\cdot}6n)(B/D), \tag{2}$$

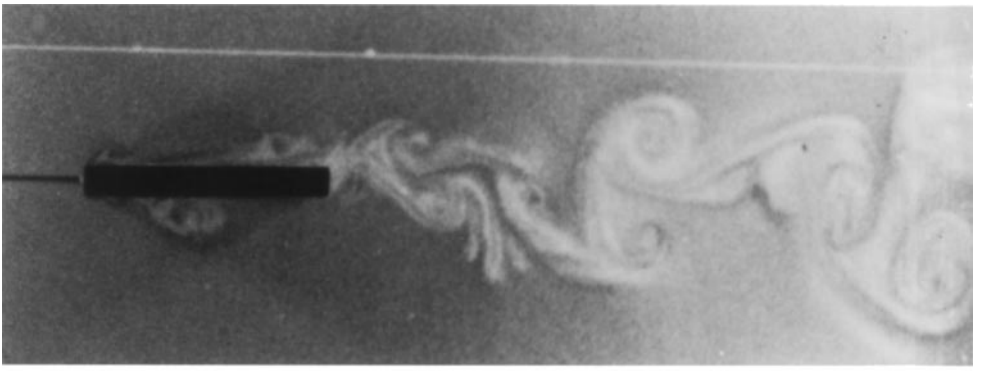

(a) 2-D Rectangular cylinder (B/D=8.2)

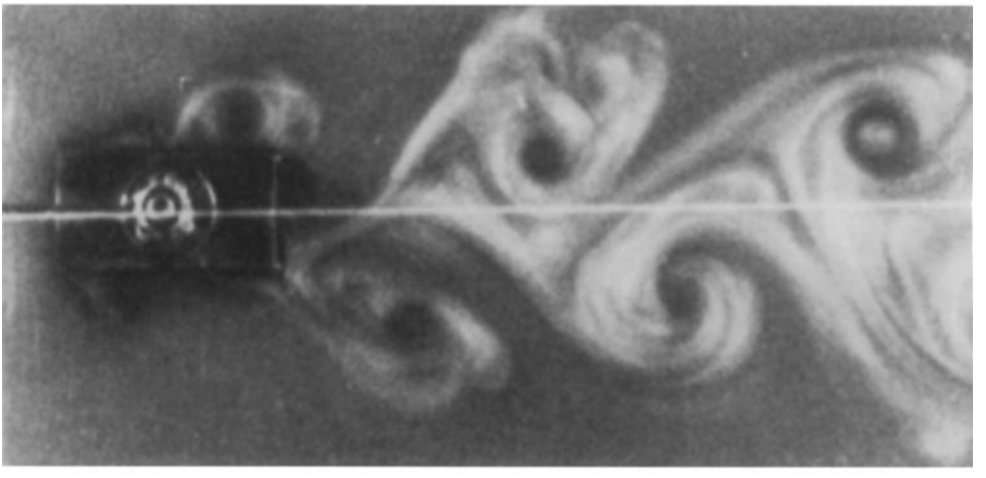

(b) 2-D Rectangular cylinder (B/D=2.0)

Figure 1. Motion-induced vortex on the side surface generated by heaving motion of (a) a 2-D rectangular cylinder ($B/D = 8{\cdot}2$), and (b) a 2-D rectangular cylinder ($B/D = 2{\cdot}0$).

where V_r is the reduced velocity ($= V/f_0D$, f_0 being the natural frequency of heaving motion, and D the body length in the cross-flow direction), and B/D the side ratio. This formula coincides with the peculiar Strouhal number proposed recently by Nakamura & Nakashima (1986), i.e. for $n = 1$,

$$\mathrm{St}^* = f_0B/V = 0{\cdot}6.$$

The reduced velocity of vortex-induced vibration, $V_r = f_0B/V$, for almost all bridge girders or fundamental structural bluff bodies, can be predicted well by equation (2) as shown in Figure 2. Some of the data show the threshold reduced velocity corresponding to $n = 2$ in equation(1), which means that the vortex generated at the leading edge convects to the trailing edge in two heaving motion cycles, and two vortices exist on the one side surface. This vortex cannot be eliminated by the installation of splitter plates in the wake (see Figure 3), which makes it clear that this vortex on the body side surface should be clearly distinguished from a Karman vortex, and that its generation is not affected by the wake flow. Furthermore, the important role of the trailing edge vortex can be confirmed by the disappearance or significant reduction of the heaving response by the installation of

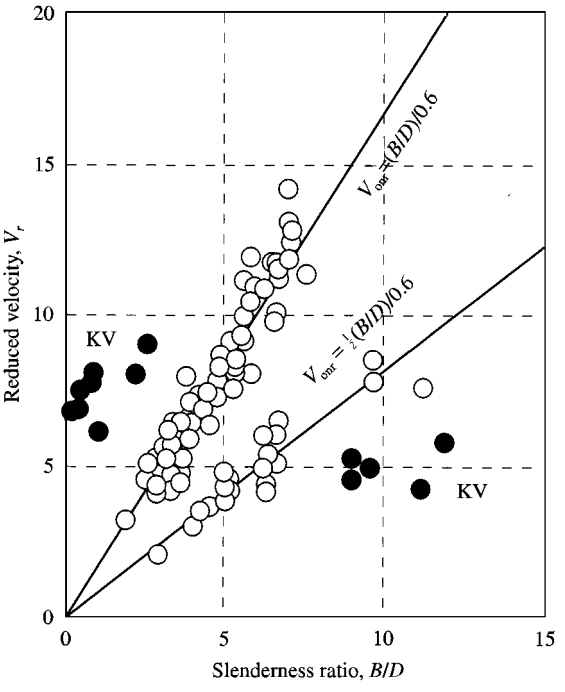

Figure 2. Reduced onset/resonance velocity (V_{onr}) for various bluff bodies (KV: caused by Karman vortex shedding).

splitter plates very close to the trailing edge, which disturbs the formation of the trailing edge vortex, as shown in Figure 3. This vortex could be generated by the enhancement of a one-shear-layer instability, by the motion itself (Komatsu & Kobayashi 1980; Shiraishi & Matsumoto 1983), or by the edge-tone effect at the body trailing edge (Nakamura & Nakashima 1986).

On the other hand, for torsional motion, a leading edge vortex with 0·6 V mean velocity, reaches the trailing edge after 1·5, 2·5, 3·5, etc., cycles of the torsional motion to coalesce with the trailing edge vortex, because the phase of the trailing edge vortex generation differs from that of the leading edge vortex for torsional motion by 180°. The reduced velocity threshold, in this case can be expressed as follows (Shiraishi & Matsumoto 1983):

$$V_{rcr} = (1/0{\cdot}6)(B/D)/(n - 0{\cdot}5), \tag{3}$$

where $n = 1, 2, 3, \ldots$.

The critical reduced velocity for the torsional vortex vibration of rectangular cylinders with $B/D = 2{\cdot}0$ can be predicted well by this formula, as illustrated in Figure 4. It is seen that the torsional response could appear when the separated vortex from the leading edge arrives at the trailing edge in a half cycle of torsional motion in order to coalesce into the secondary vortex generated at trailing edge.

A particular case of the torsional response is shown in Figure 5. If the rotational axis is fixed behind the trailing edge of a rectangular cylinder with $B/D = 4$, then the torsional response occurs at two different reduced velocities. These characteristics clearly show that two different vortex excitations exist, i.e. the one-shear-layer vortex-related response characterized by equation (3) and the Karman vortex excitation defined by the reciprocal of the Strouhal number. A splitter plate in the wake can suppress the second response due to the

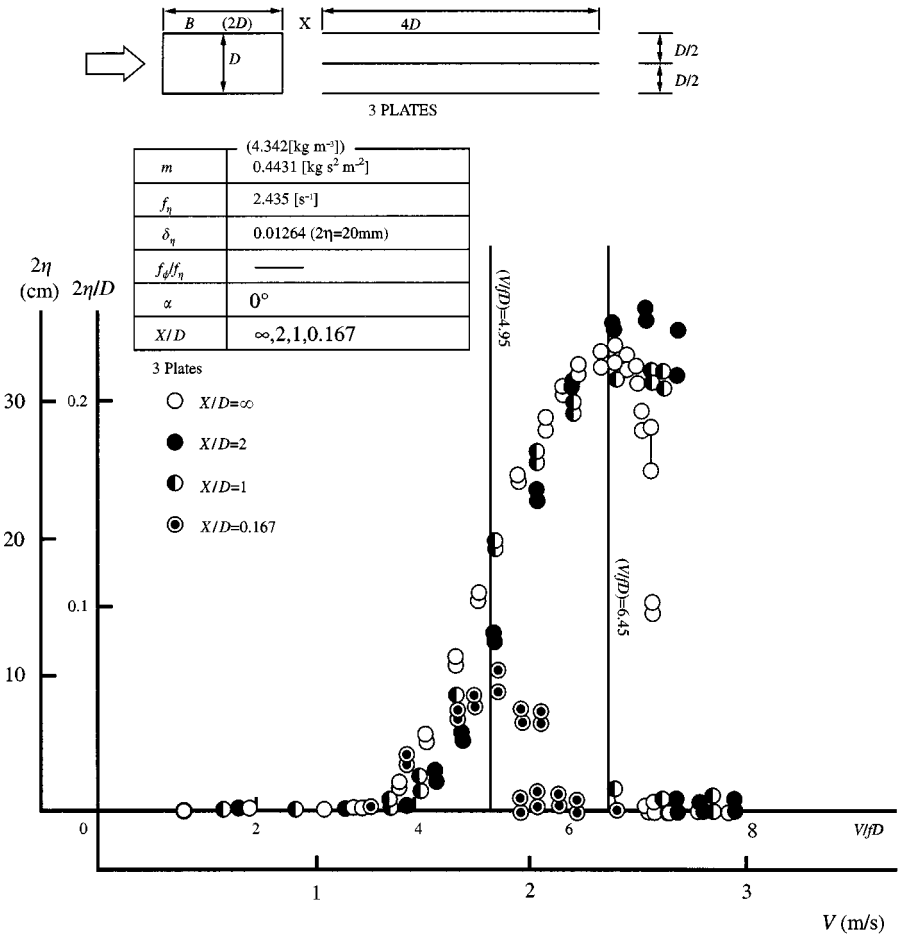

Figure 3. Effect of splitter plate(s) in a wake on vortex-induced oscillation (heaving motion) for a 2-D rectangular cylinder with $B/D = 2{\cdot}0$, in smooth flow.

Karman vortex and alternatively amplify the first response due to the one-shear-layer vortex, as shown in Figure 5 (Shiraishi & Matsumoto 1983).

In order to suppress or mitigate the velocity-restricted response caused by the one-shear-layer related vortex, the control of the generation of the leading edge vortex caused by body motion is essential, and a suitable modification of the leading edge geometrical shape, e.g. by the installation of edge fairing, wind noses, deflectors, flap plates and so on, is often used as an aerodynamic countermeasure. On the other hand, increasing the Scruton number ($\mathrm{Sc} = 2m\delta/\rho D^2$, where m is the mass per unit length, δ the structural damping, ρ the air density, D the body dimension) for structures is also effective for response mitigation; therefore, some damping devices have been installed inside or under bridge decks.

3. VORTEX ENHANCED BY APPLIED SOUND

A vortex could be generated by the enhancement of shear-layer instability by sound. Parker & Welsh (1983) reported the effect of sound on the flow pattern on the side surface of

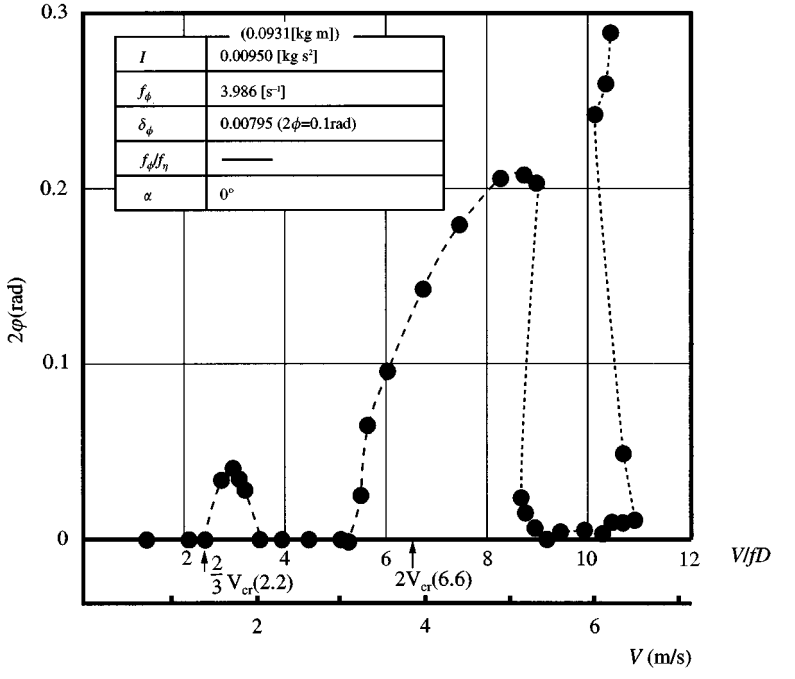

Figure 4. Torsional vortex-induced oscillation for a 2-D rectangular cylinder with $B/D = 2{\cdot}0$.

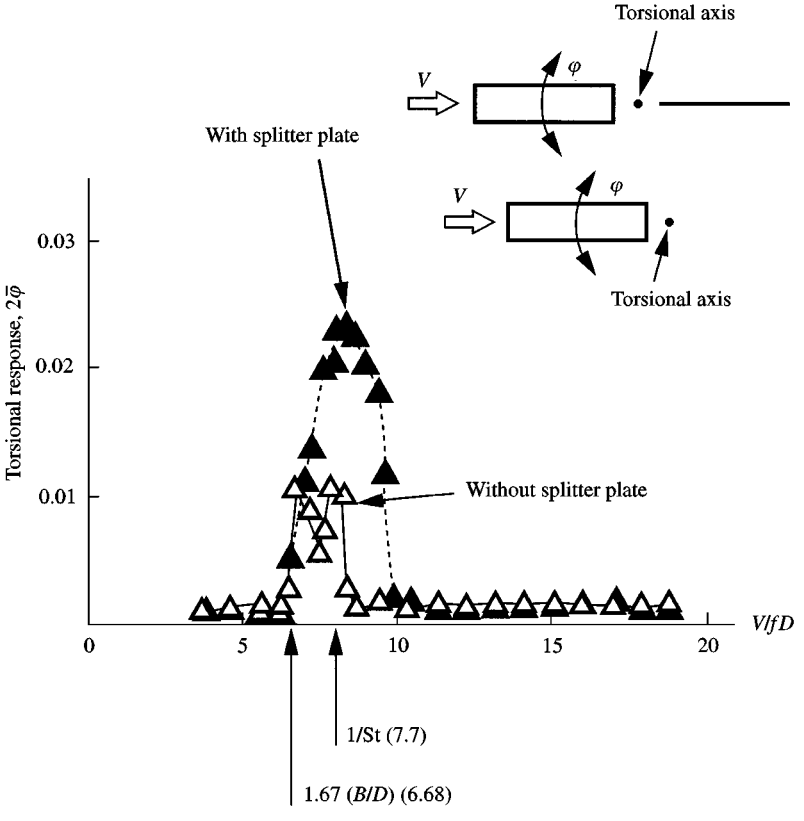

Figure 5. Torsional vortex-induced oscillation of 2-D rectangular cylinder with $B/D = 4{\cdot}0$ without/with a splitter plate in a wake.

rectangular cylinders with various side ratios. The applied sound technique is useful for the evaluation of bridge girder sensitivity to vortex-induced vibration. For example, instead of the direct measurement of the response of box sections or girders in an elastically supported system, the unsteady pressure measurement on the stationary girder side-surface with the application of sound on the side-surface from the ceiling and the floor of a wind tunnel, can be used to evaluate the instability grade of the bridge girder to vortex-induced vibration. If the unsteady pressure, with the frequency synchronized to the applied sound frequency on the stationary body side-surface, is significantly enhanced at the specified reduced frequency where the vortex-induced vibration appears, then this body must show a significant vortex-induced vibration. In other words, the instability/stability grade of bluff bodies in relation to vortex-induced vibration can be evaluated by the sensitivity of unsteady pressure on the stationary body side-surface to the applied sound, with the great advantage of a significant time saving in comparison to testing of elastically supported bodies. An example of such a test result is shown in Figures 6(a) and 6(b), in which the V (velocity) versus A (amplitude of heaving response) diagrams are compared with the PSD of unsteady pressure on a stationary body side-surface (Matsumoto *et al.* 1991).

4. SYMMETRICAL VORTEX-SHEDDING ENHANCED BY LONGIDUDINALLY HARMONICALLY FLUCTUATING FLOW

The symmetrical vortex shedding for a circular cylinder in the range of a quarter the reduced velocity corresponding to the reciprocal of the Strouhal number was visualized by King (1977). This symmetrical vortex shedding might excite longitudinal response at comparatively low wind velocity; therefore, the detailed understanding of this vortex-induced vibration is important in the design of flexible structures. Figure 7(a) shows the symmetrical vortex shedding for a 2-D rectangular cylinder with $B/D = 0{\cdot}5$ under the longitudinally harmonically fluctuating flow, whose r.m.s. value was less than 0·01 of the mean oncoming flow velocity, at the specified reduced velocity, characterized by the fluctuating flow frequency of a quarter of 1/St where St is the Strouhal number (Knisely *et al.* 1986). In addition to the symmetric vortex shedding at this velocity, the highly amplified Karman vortex shedding, which rolled up very strongly and very closely to the cylinder rear surface in the wake, was intermittently observed as shown in Figure 7(b). The intensive Karman vortex shedding could make the drag force larger than in a smooth flow (Matsumoto *et al.* 1984).

The elastic wind tunnel model of the horizontal twin beams with rectangular sections of a giant crane, showed an in-line vortex vibration at a specified reduced velocity of 1/4S1, and seemed to be caused by this kind of the symmetrical vortex shedding(Shiraishi & Matsumoto 1981).

5. VORTEX SHEDDING CHARACTERISTICS OF 2-D RECTANGULAR CYLINDERS WITH 0·5 SIDE-RATIO DEPENDING ON THE ANGLE OF ATTACK

The flow pattern around the body characterizes its aerostatic and aerodynamic features. A 2-D rectangular cylinder with $B/D = 0{\cdot}5$ changes its aerostatic and aerodynamic characteristics with the angle of attack. Figures 8, 9 and 10 show the test results of the Strouhal number (S1), the lift force coefficient (C_L), and the drag force coefficient (C_D) versus the angle of attack (α or $\beta = 90^\circ - \alpha$). From these results, it is seen that the characteristic values change suddenly at the particular angle of attack of $\alpha = 23$ and 83° (Matsumoto *et al.* 1988).

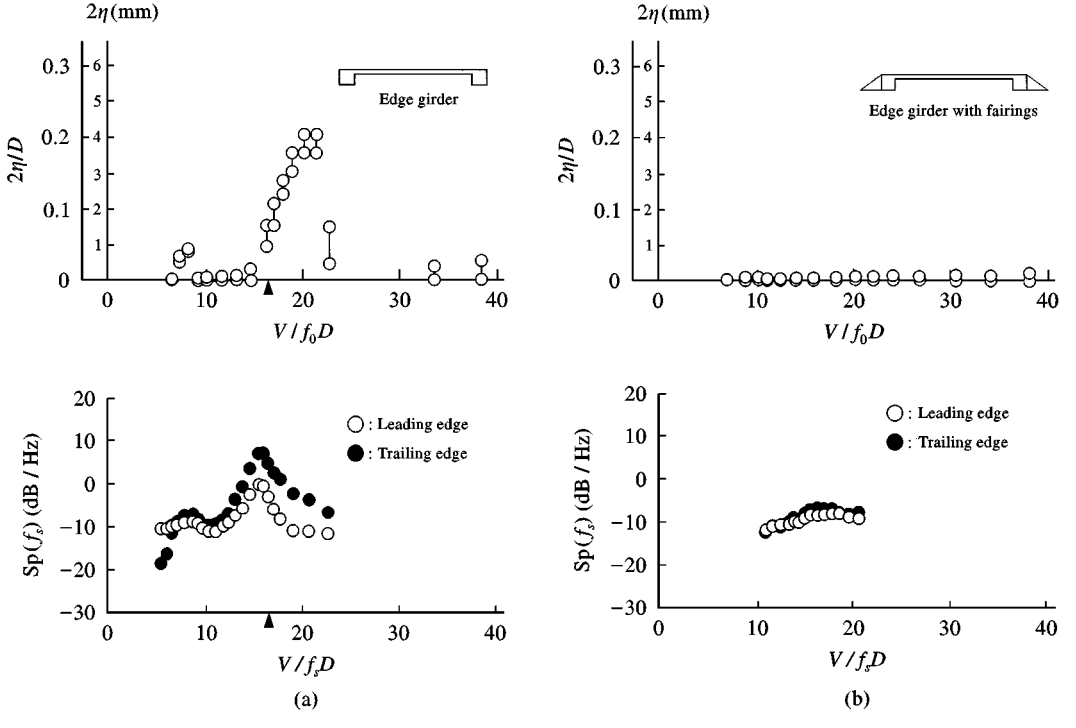

Figure 6. Correspondence of unsteady pressure on side surface of a stationary edge girder under applied sound to the vortex-induced oscillation in smooth flow without sound. The power at $f = f_s$ of PSD of unsteady pressure of near leading and trailing edge on side surface for stationary edge girder under applied sound (f_s: applied sound frequency); Sp stands for spectrum. (a) For plain edge-girder; (b) for girder with fairings.

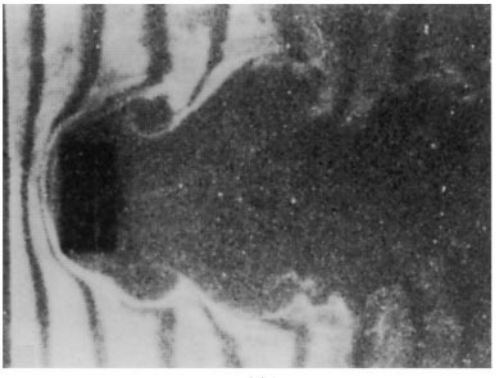

(a)

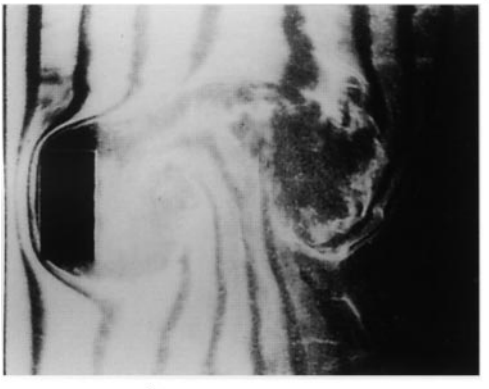

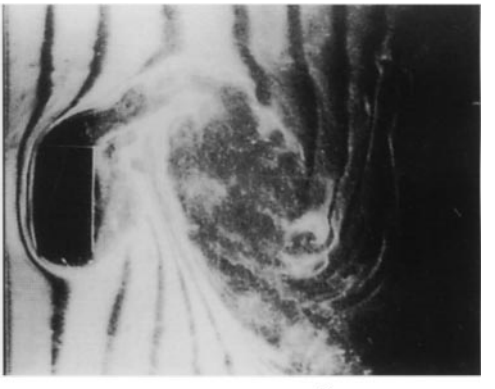

$f_p = 0$ (no disturbance) (b) Enhance vortex shedding at f_pD/V=4St (with distrurbance (f_p: pulsating flow frequency)

Figure 7. (a) Symmetric vortex shedding synchronized to the pulsating frequency ($f_pD/\bar{V} = 4\text{St}$). (b) The Karman vortex shedding (alternat asymmetric vortex shedding).

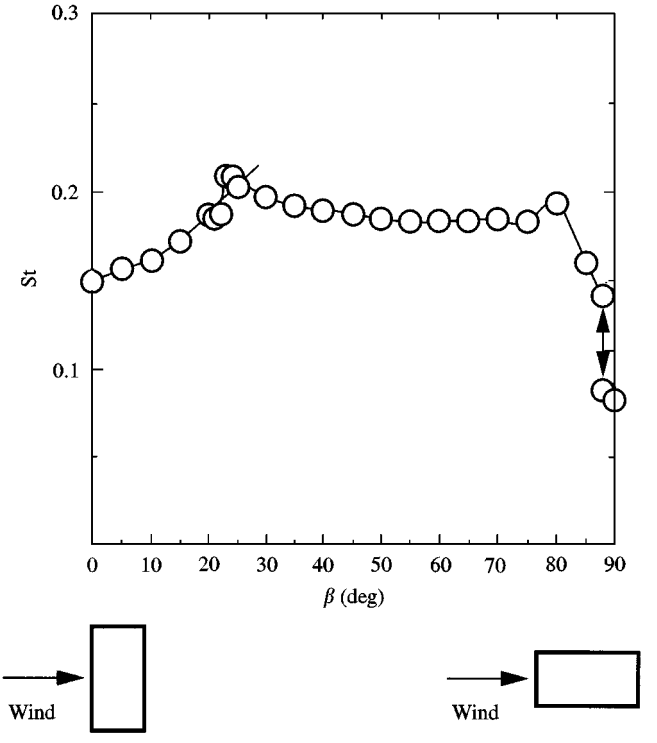

Figure 8. Strouhal number, St, versus the angle of attack β for 2-D rectangular cylinder with $B/D = 0{\cdot}5$.

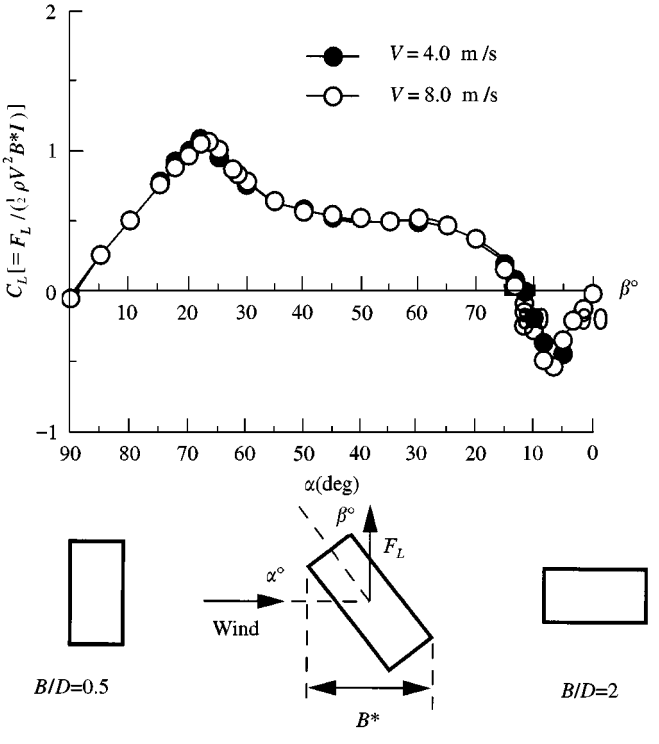

Figure 9. Lift coefficient C_L versus the angle of attack β for 2-D rectangular cylinder with $B/D = 0{\cdot}5$.

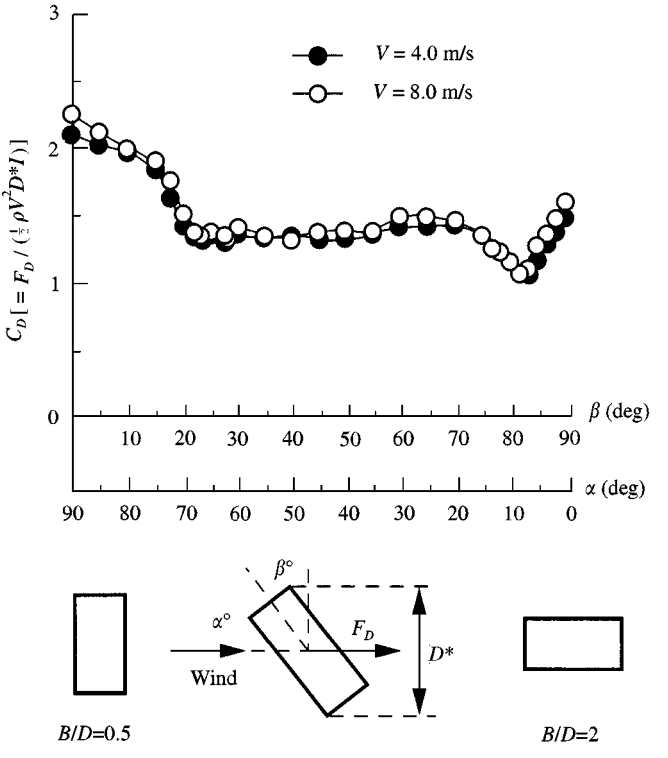

Figure 10. Drag coefficient for various β (2-D rectangular cylinder with $B/D = 0{\cdot}5$).

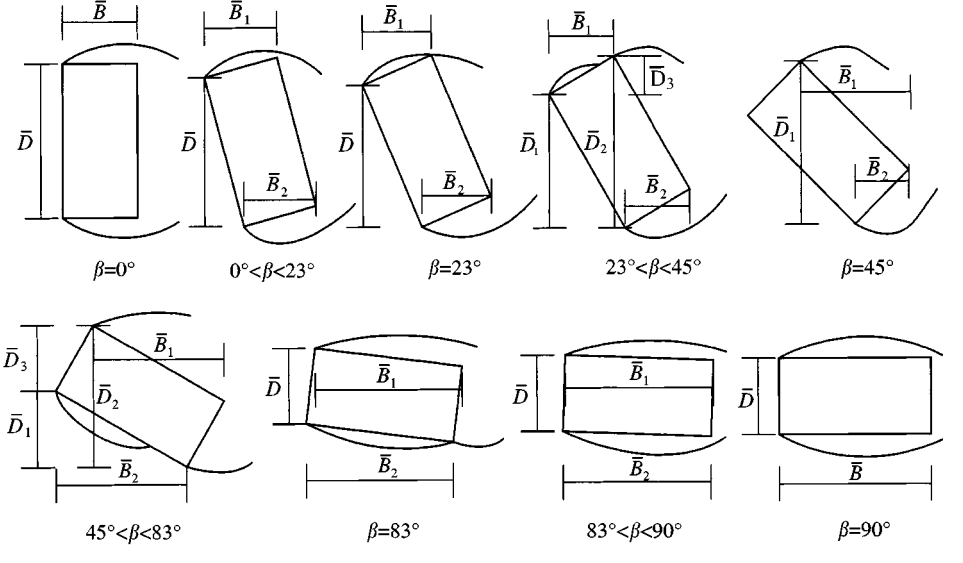

Figure 11. Illustration of flow separation depending on β (2-D rectangular cylinder with $B/D = 0{\cdot}5$).

The reason for these characteristics can be explained by the change of the time-average flow pattern, depending upon the angle of attack, as illustrated in Figure 11.

Furthermore, the vortex-shedding characteristics were also investigated by the applied sound method. The same kinds of vortices as those by the applied sound were enhanced at a specified reduced frequency. The amplitudes of the fluctuating lift force coefficient (C_L) and the drag force coefficient (C_D), which are synchronized to the applied sound frequency, are illustrated as the function of the reduced velocity, characterized by the sound frequency, in Figure 12(a) (for the lift force) and Figure 12(b) (for the drag force) for $\alpha = 0, 15, 23, 35, 45, 60, 75, 83, 88$ and 90°. The local peaks in these diagrams are due the enhancement of the vortex-shedding/generation, where the local peaks of the lift force at 1/S1 and $1{\cdot}67\bar{D}/\bar{B}$ correspond to the Karman vortex-shedding and the one-shear-layer related vortex generation, respectively. On the other hand, the local peaks of the drag force at 1/S1 (because of the out-of-phase sound stimulation in this test) and 1/4S1 correspond to the Karman vortex-shedding and the symmetrical vortex-shedding, respectively. In summary, for $0^\circ < \alpha < 23^\circ$, the Karman vortex-shedding, the symmetrical vortex-shedding and the one-shear-layer instability-related vortex generation, could appear. For $23^\circ < \alpha < 83^\circ$, only Karman vortex-shedding exists and for $83^\circ < \alpha < 90^\circ$, the Karman vortex, the symmetrical vortex-shedding and the one-shear-layer instability-related vortex generation could exist apparently or latently for some vortices.

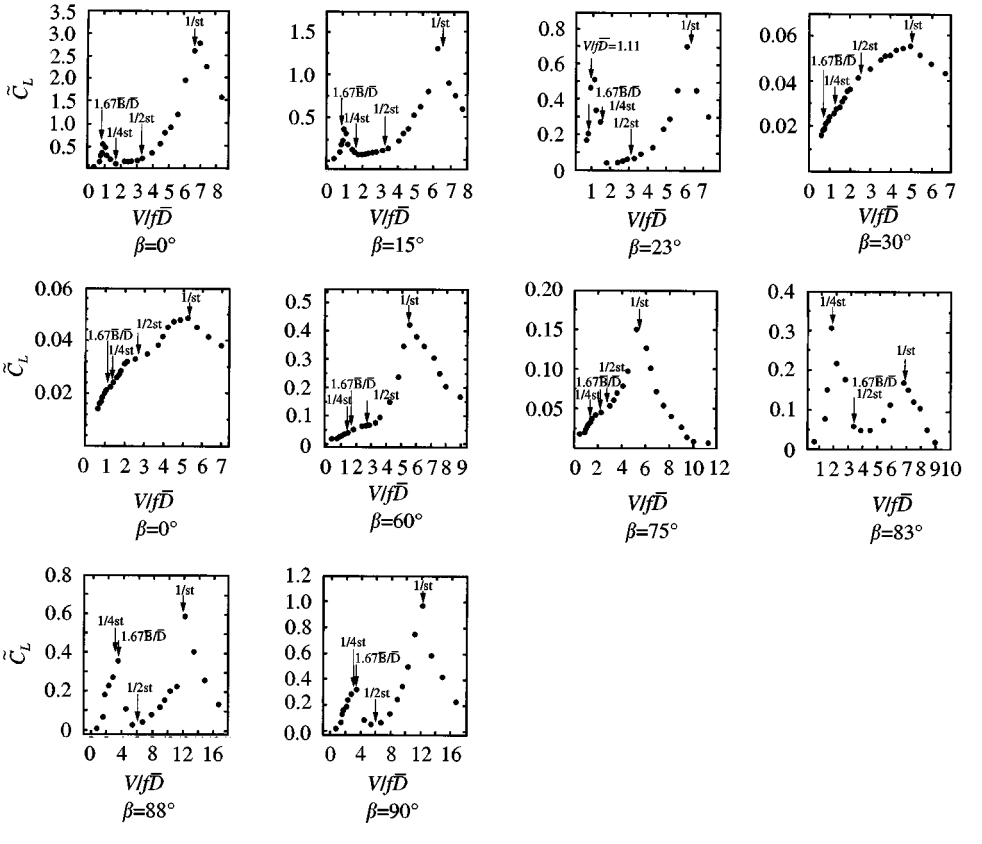

Figure 12(a). Fluctuating life coefficient, synchronized with the out-of-phase applied sound, for stationary 2-D rectangular cylinder with various $\beta(B/D = 0{\cdot}5)$.

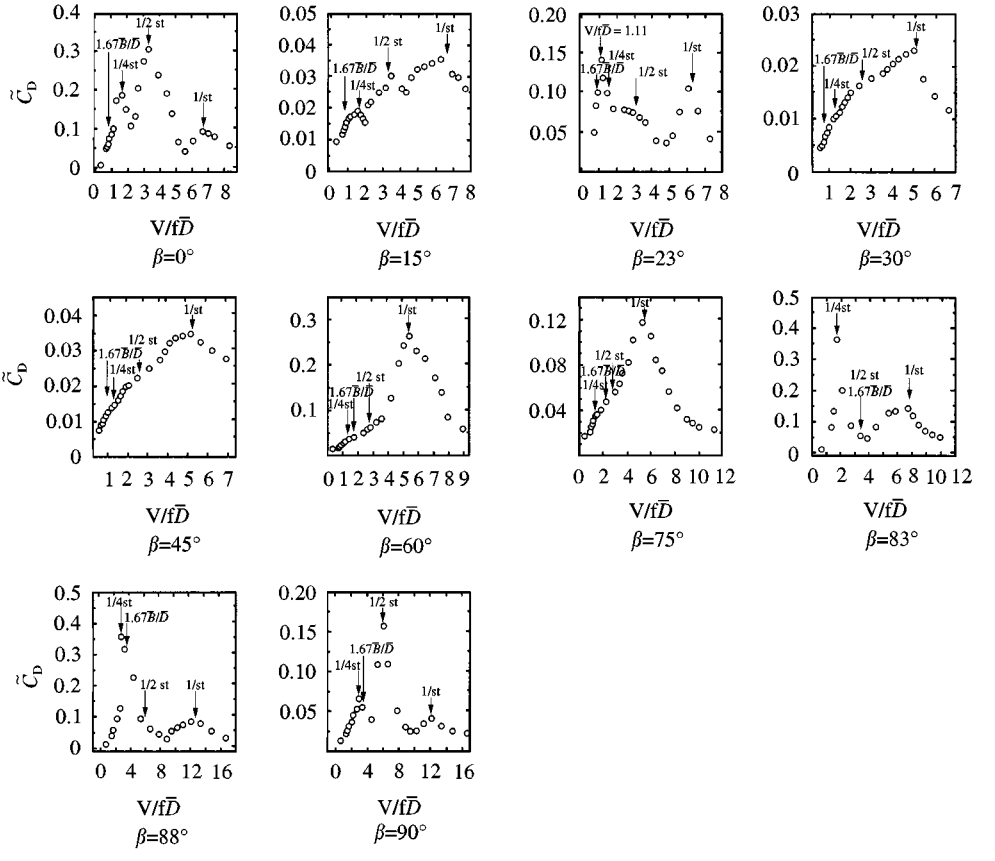

Figure 12(b). Fluctuating drag coefficient, synchronized with the out-of phase applied sound, for stationary 2-D rectangular cylinder with various $\beta(B/D = 0{\cdot}5)$.

6. THE AXIAL VORTEX BEHIND AN INCLINED CABLE AND THE TIP VORTEX FROM THE FREE END OF TOWER STRUCTURES

Inclined cables of cable-stayed bridges have often shown violent vibration on windy and rainy days, which has become a major issue for the bridge designers nowadays. This cable vibration is often observed on rainy days, therefore it is called "rain vibration" or "rain- and wind-induced vibration". Based upon many experiences to-date, the following conditions ought to be satisfied for the appearance of this type of cable vibration: a wind velocity range of 5–15 m/s, in the subcritical Reynolds number range, in a skew wind direction to the bridge axis, for the downstream side cables behind a bridge tower, for cables lapped by polyethylene, in comparatively low-turbulence wind, and so on. These conditions are not always essential; for example, a few cable vibrations were observed not on rainy days but on fine or cloudy days, at a high wind velocity (for example 40 m/s), on the upstream cables of a bridge tower, for other cable surface conditions such as FRP (fibre resin pipe), and so on (Matsumoto *et al.* 1992).

In a wind tunnel, the inclined/yawed cable model without a water rivulet on the cable surface, therefore with a smooth cable surface, showed a galloping instability in smooth flow, which was clarified to be caused by the axial flow at the near wake of the

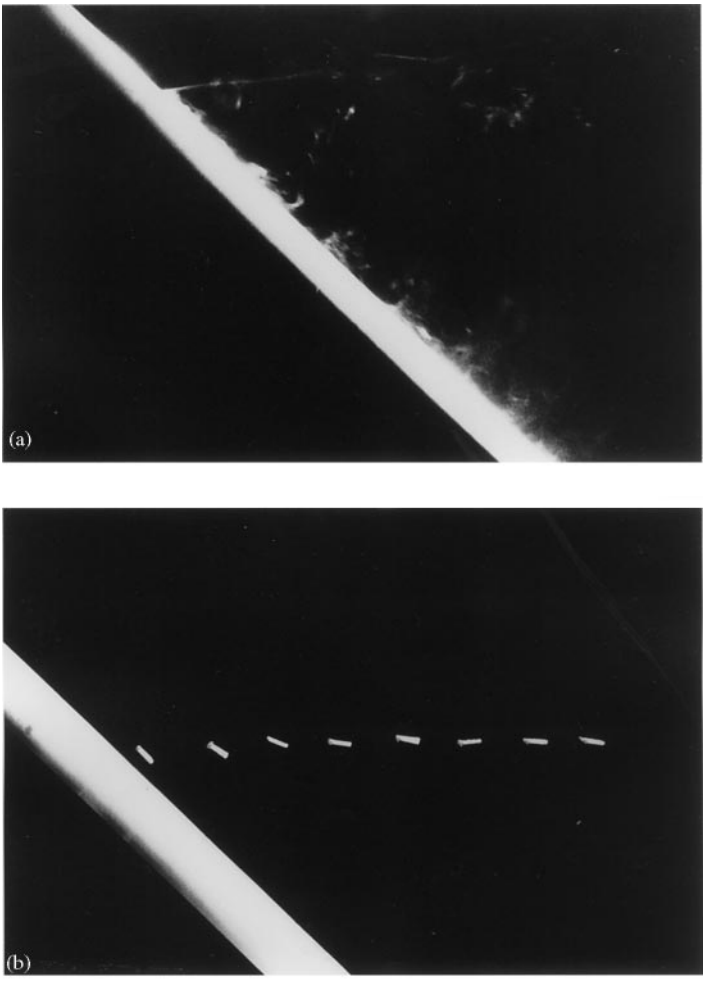

Figure 13. Flow visualization of the axial flow for inclined cable with $\beta = 45°$; the flow comes from the left-hand side. Visualization by (a) liquid paraffin, and (b) by light small flags.

inclined/yawed cable, as visualized in Figure 13 (yawed cable with $\beta = 45°$ in a smooth flow). This axial flow causes the negative slope of the lift force, which was confirmed by the lift force measurement for the nonyawed cable with an artificial flow in the near wake (see Figure 14 for a smooth-surface cable with $\beta = 45°$ in a smooth flow), and the axial flow velocity is almost equal to the approach flow velocity at $\beta = 45°$ (Matsumoto *et al.*1992). Furthermore, the upper water rivulet on a cable surface causes the negative slope of the lift force as shown in Figure 15, where a thin tape modelled the water rivulet and where its location from the front flow stagnation point is denoted by θ in this figure. The aerodynamic instability depends sensitively on the location of the upper rivulet. However, both V (velocity) versus A (response amplitude) and δ (aerodynamic logarithmic damping) diagrams (see Figure 16: the yawed smooth surface cable with $\beta = 45°$ in a smooth flow) and the unsteady lift force coefficient diagrams in terms of aerodynamic damping (see Figure 17: the yawed and smooth surface cable with $\beta = 45°$ a smooth flow) clearly indicate the velocity-restricted response at certain specific reduced velocity ranges, which are

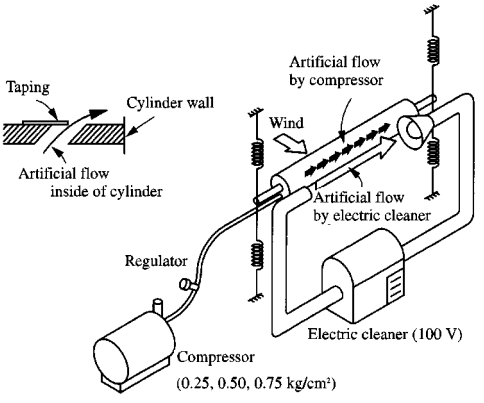

Artificial axial flow generator

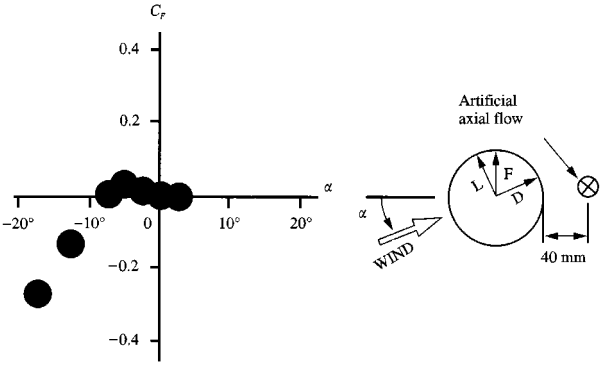

Figure 14. Lateral force coefficient characteristic of nonyawed cylinder with artificial axial flow (in smooth flow).

comparatively higher than the resonance reduced velocity with Karman vortex-shedding; they seem to be certain multiples of 20, such as 40, 80 and so on.

Because, in the V–A–δ diagram, the existence of vortex-induced vibration can be known by both of the appearance of a response and the drastic change of aerodynamic damping, in the velocity axis and in an H_1^* diagram the local positive velocity axis means the aerodynamically unstable range.

Furthermore Figure 18 shows the enhanced velocity fluctuation in the wake, synchronized to the cable vibration frequency, under a forced cross-flow vibration with a stationary amplitude, at the specific reduced velocity which corresponds to the response appearance. This fact clearly implies the existence of a certain vortex-shedding at such a higher reduced velocity range; in other words, with a much longer period than that of the conventional Karman vortex-shedding (Matsumoto 1998).

The cable response accelerations of Meiko West Bridge I (old bridge) and Bridge II (new one), with the main span length of both bridges 405 m, have been measured by the Japan Highway Authority. Some examples of the unsteady power spectra obtained by wavelet analysis of the cable response are shown in Figure 19 (for the Old Bridge) and Figure 20 (for the New Bridge) (Matsumoto 1998). The former result shows the typical beating characterstics, which have been observed for many old and new bridges. In the response shown in

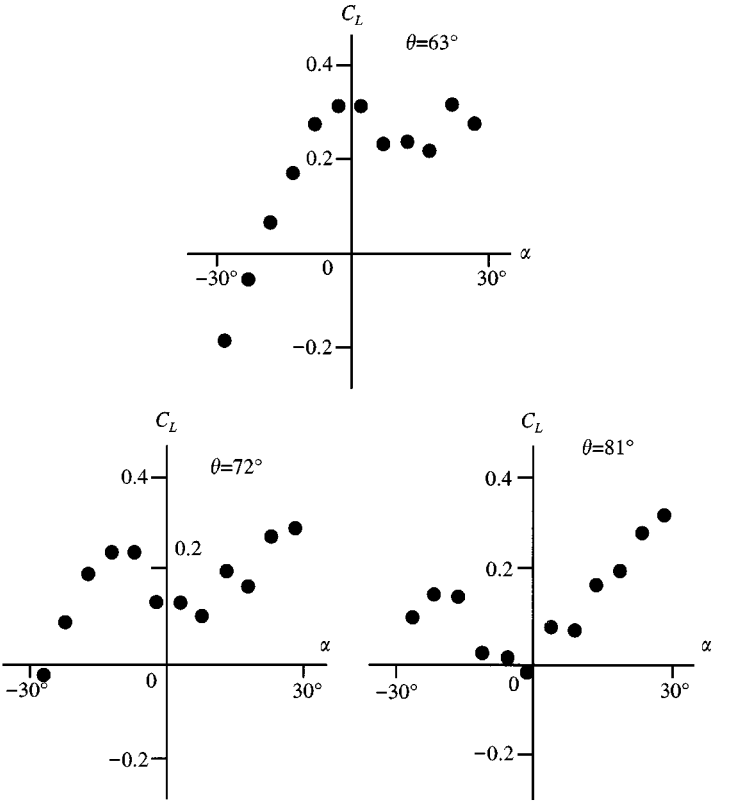

Figure 15. Lateral force coefficient of yawed cable ($\beta = 45°$) with artificial upper rivulet (in smooth flow).

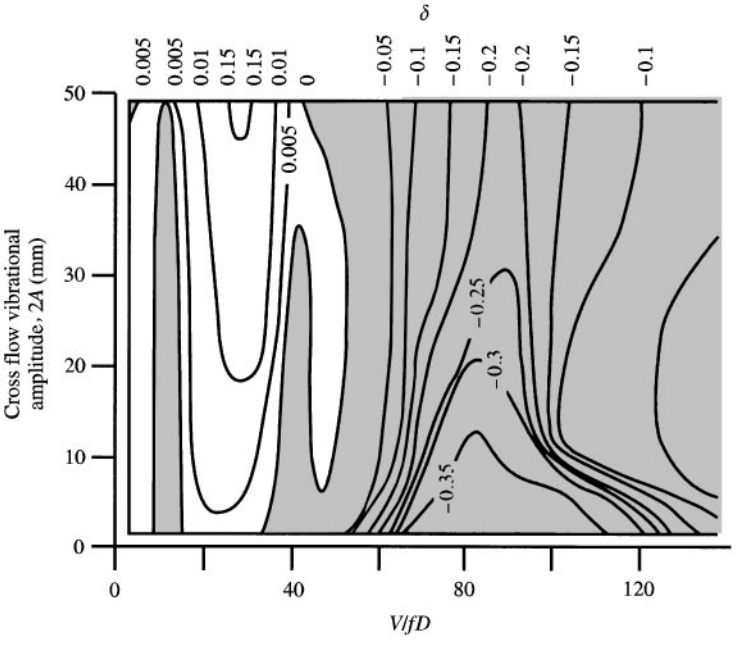

Figure 16. Velocity (V) versus amplitude (A) and damping (δ) diagram for a yawed cable with rivulet (vertical angle $\alpha = 0°$, yaw angle $\beta = 45°$, location of artificial upper rivulet measured from the front flow-stagnation $\theta = 72°$).

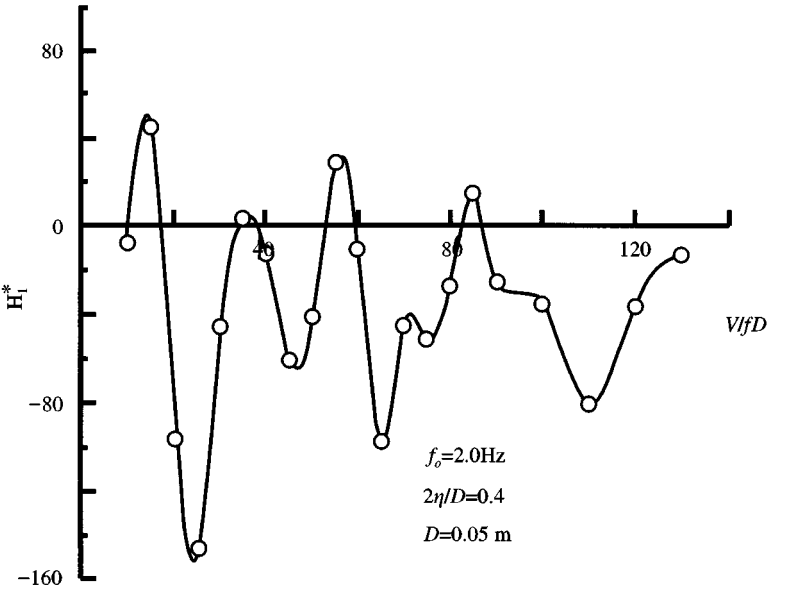

Figure 17. Unsteady lift force coefficient, H_1^*, related to aerodynamic damping for a cable with rivulet ($\theta = 63°$) in smooth flow.

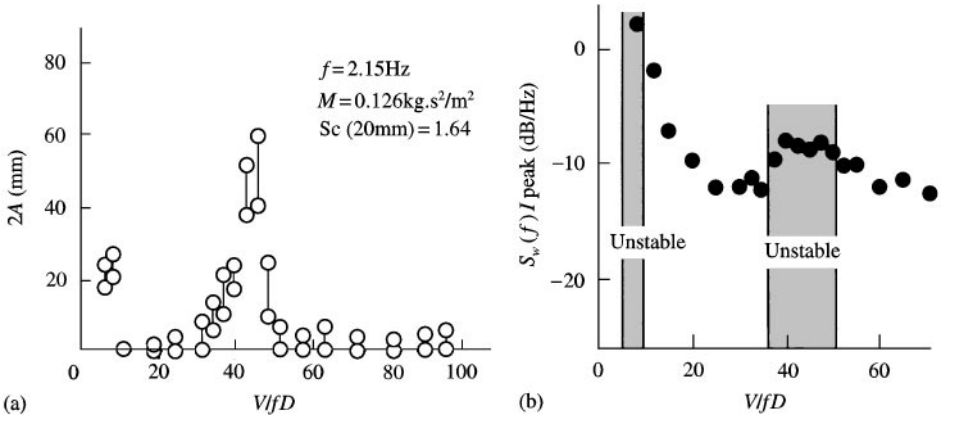

Figure 18. (a) Velocity-amplitude diagram and (b) the power of the fluctuating velocity in a wake synchronized to heaving forced motion of the yawed cable ($\beta = 35°$) with rivulet ($\theta = 58°$).

Figure 19, the beat response occurred with the 4th and the 5th modes of the inclined cable, whose reduced velocities corresponded to 32 and 25, respectively. Furthermore, the long period of the peak-to-peak amplitudes of the beat response corresponds to a reduced velocity of approximately 120. It should be noted that the inclined cables are apt to show a beat response with a suitable combination of modes in the way that the long period of the beating vibration might correspond to characteristic reduced velocity ranges, such as 20, 40, 60, 80, 100, 120, and so on. Also in Figure 19, the nonstationary peak appears locally at the specified reduced velocity ranges of 40 and 80. On the other hand, in a few cases, even a comparatively steady response could be observed, as shown in Figure 20 for the new bridge. The 3rd mode vibration appeared at the reduced velocity range of around 20.

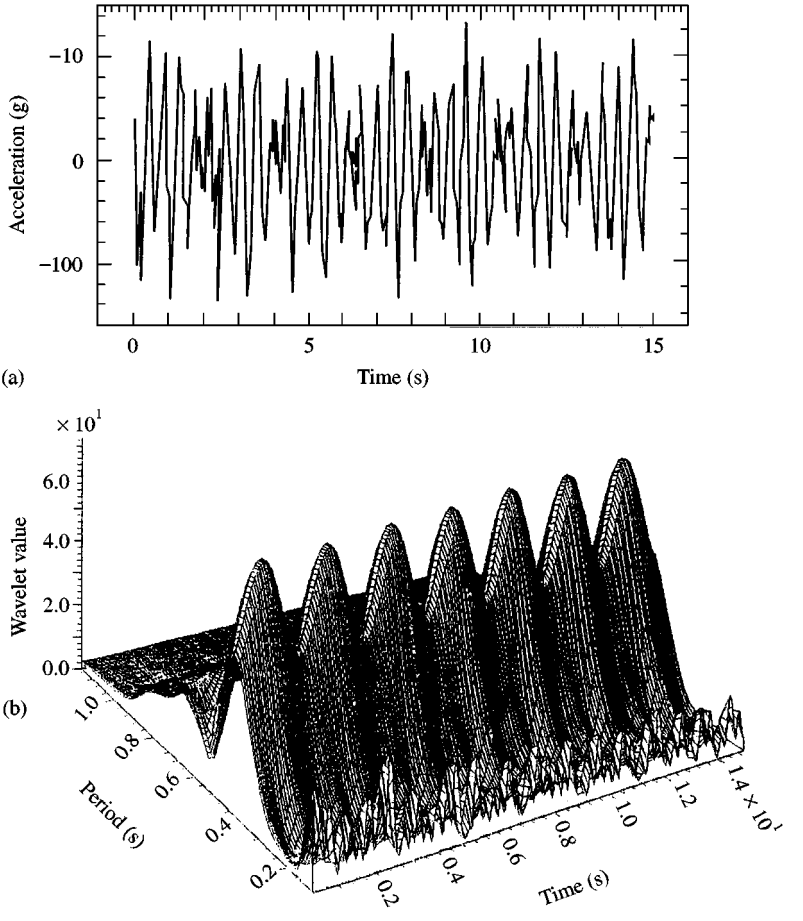

Figure 19. Observed beat response of Meiko Old Bridge: (a) time trace; (b) wavelet analysis.

The reason for the velocity-restricted response at the high-reduced velocity is unfortunately not sufficiently clarified yet, but a certain vortex with a long period, which would be generated by the complex flow field around the inclined cable, surely excites the inclined cable. Figure 21 shows the flow pattern around a yawed smooth surface cable model with $\beta = 45^\circ$ in a smooth flow, visualized by the fluid paraffin method, in which a vortex along the cable axis, so called "axial vortex", can be observed. In particular, it seems that the Karman vortex-sheds more strongly once every three vortex-sheddings, which must be related to the "axial vortex". This intermittent amplification of the Karman vortex-shedding can clearly be found in the unsteady lift force diagram and the fluctuating velocity diagram, obtained by wavelet analysis, and in the wake of the yawed ($\beta = 45^\circ$) cable model with a smooth surface, as shown in Figures 22 and 23, respectively. On the other hand, Durgin *et al.* (1980), Shirakashi *et al.* (1985) and Nakagawa *et al.* (1983) reported that the peak appeared at the PSD of the fluctuating velocity in the wake of an inclined circular cylinder at the specified frequency corresponding to a higher-than-the-reciprocal-of-Strouhal-number reduced velocity of 2·8 (by Durgin) or 3·0 (by Shirakashi), i.e. approximately 20. Their reports must be fundamentally identical to the one on inclined cable aerodynamics discussed above.

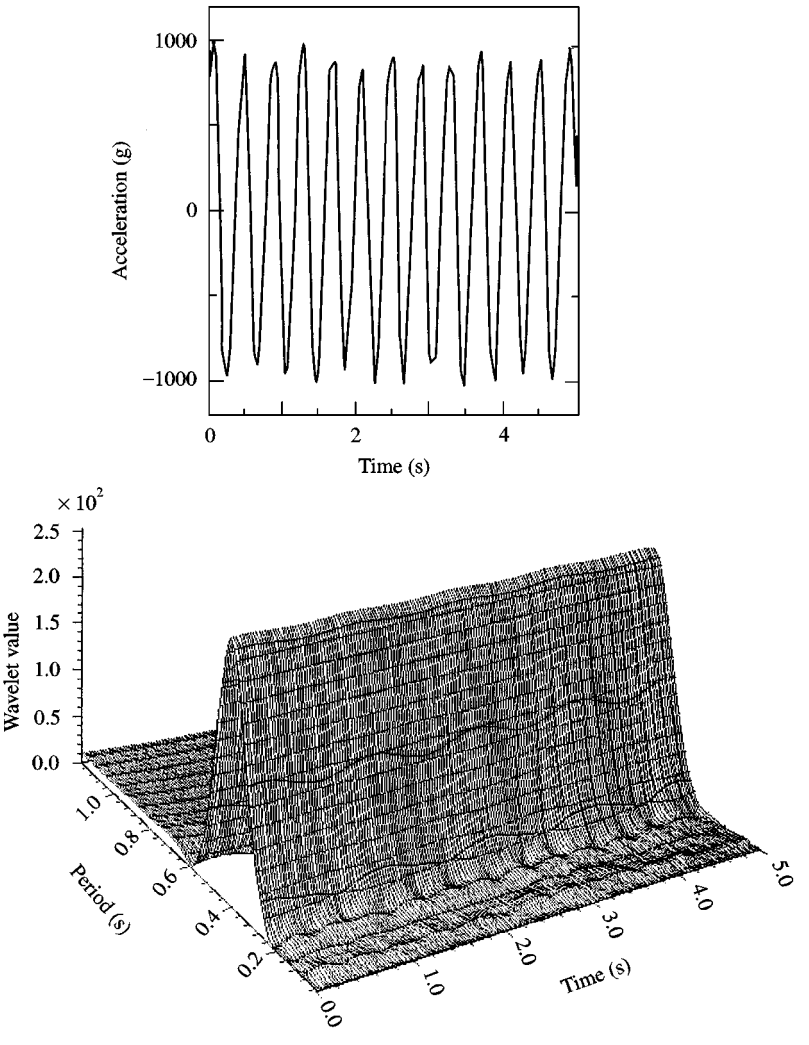

Figure 20. Observed single mode vibration of Meiko New Bridge: (a) time trace; (b) wavelet analysis.

Furthermore, Kawai (1996) and Kitagawa *et al.* (1997) discussed the appearance of a similar phenomenon for a tapered circular tower or a circular tower at around $V_r = 20$. Kitagawa *et al.* (1997) suggested this response would cause a certain vortex near the top of the tower, the so-called "tip vortex". The "tip vortex" must also be generated by complex three-dimensional flow. The detailed mechanisms of the "axial vortex" of an inclined cable and the "tip vortex" should be investigated in more detail in further studies.

7. CONCLUSION

In this paper, the various types of vortex generation around bluff bodies are introduced and discussed; however, their mechanisms are not always sufficiently clear as yet. More detailed tests, with various highly advanced techniques or with the aid of CFD, would be essential for the clarification of these complex mechanisms.

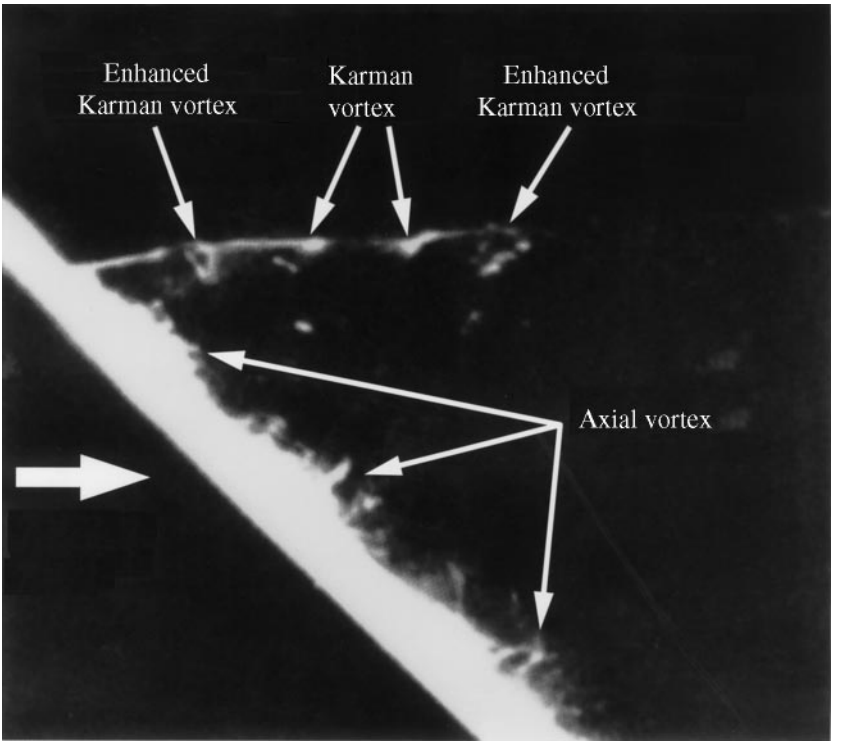

Figure 21. Visualized axial vortex by liquid paraffin around yawed cable ($\beta = 45^\circ$).

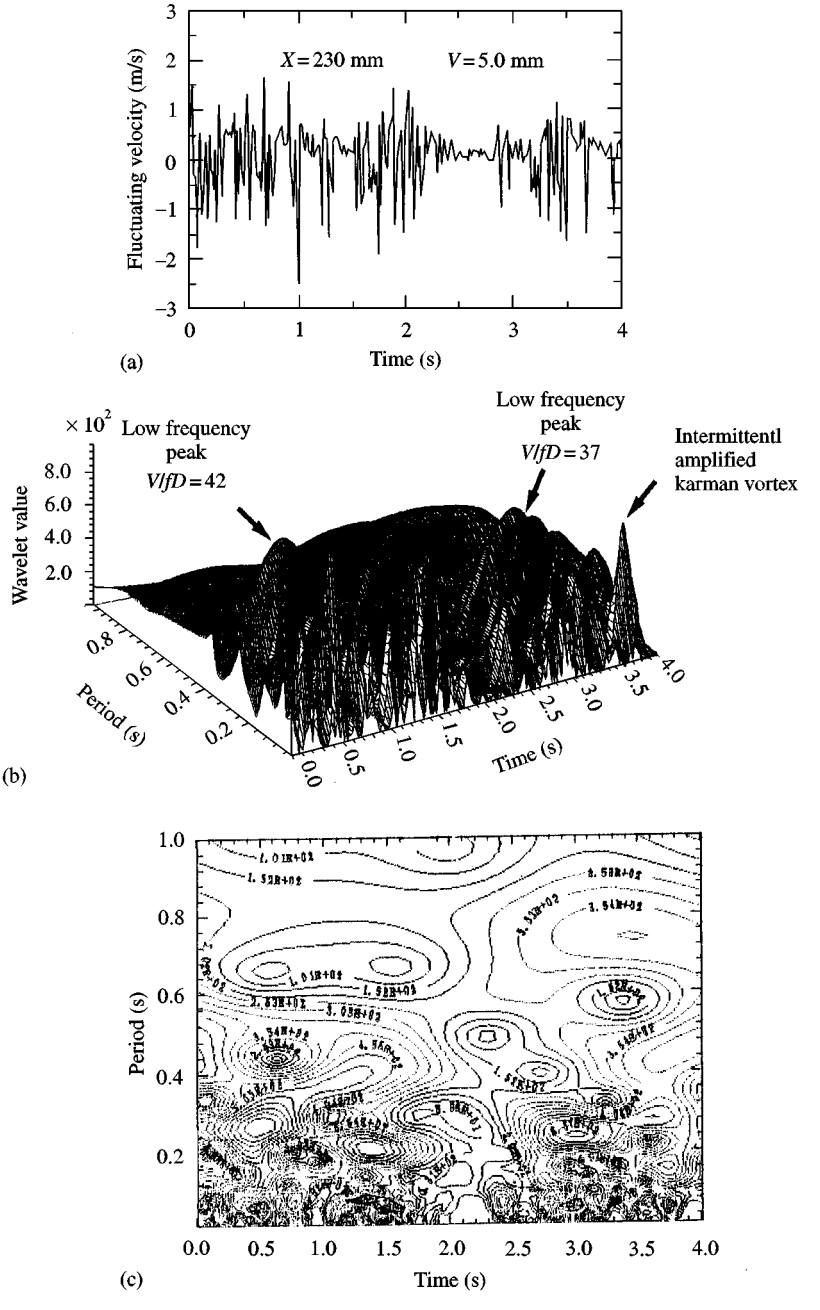

Figure 22. (a) Unsteady fluctuating velocity in a wake of the stationary yawed cable ($\beta = 45°$) and (b,c) the wavelet analyzed results ($V = 5{\cdot}0$ m/s).

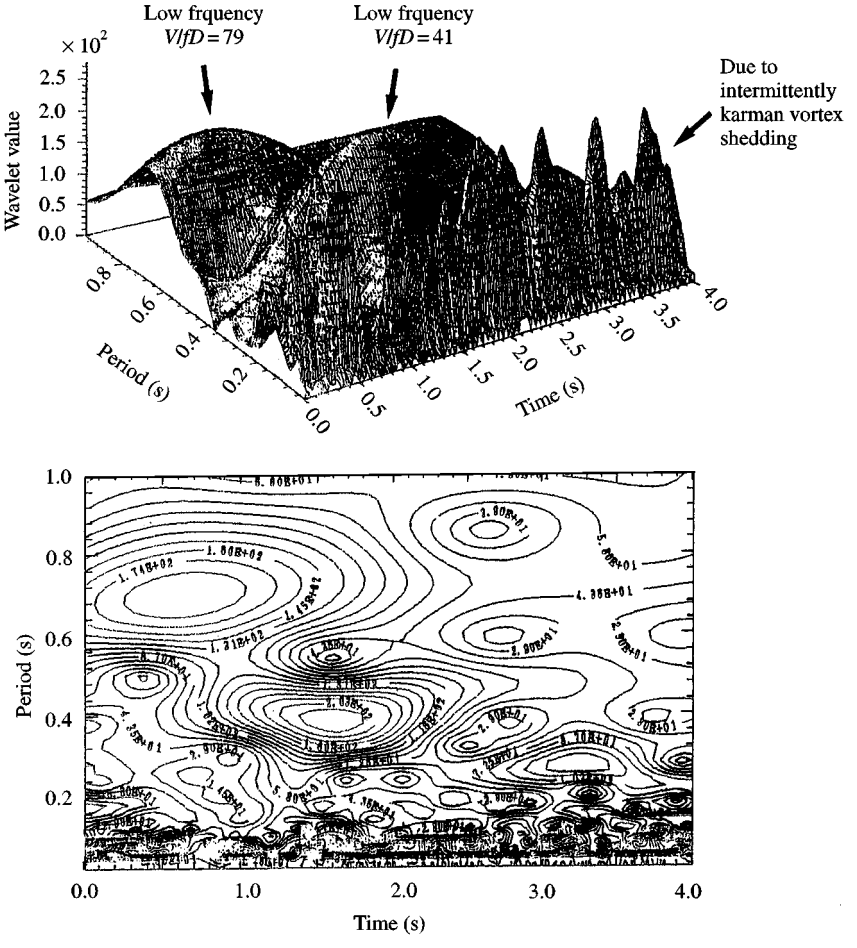

Figure 23. Unsteady lift force of the stationary yawed cable (wavelet analysis).

References

Bearman P. W. & Trueman D. M. 1972 An investigation of the flow around rectangular cylinders. *The Aeronautical Quarterly* **23,** 229–237.

Durgin W. W., March P. A., & Lefebvre P. J. 1980 Lower mode response of circular cylinder in cross-flow. *ASME Journal of Fluids Engineering* **102,** 183–190.

Kawai H. 1996 Vortex induced vibration of tapered cylinders. *Journal of Wind Engineering, JAWE*, **59,** 49–52 (in Japanese).

King R. 1977 A review of vortex-shedding research and its application. *Ocean Engineering* **4,** 141–171.

Kitagawa T., Fujino Y., & Kmura, K. 1997 An experimental study on vortex-induced vibration of circular cylinder tower at a high wind speed. *Journal of Wind Engineering and Industrial Aerodynamics* **69–71,** 731–744.

Knisely C., Mtsumoto M., & Menacher F. 1986 Rectangular cylinder in flows with harmonic perturbations. *ASCE Journal of Hydraulic Engineering* **112,** 690–704.

Komatsu S., Kbayashi, H. 1980 Vortex-induced oscillation of bluff cylinders. *Journal of Wind Engineering and Industrial Aerodynamics* **6,** 335–362.

Matsumoto, M., Kisely, C. & Menarcher, F. 1984 On flow pattern and fluid characteristics of rectangular prism in unsteady flow. *Proceedings of the 8th National Symposium on Wind Engineering*, pp. 263–270 (in Japanese).

MATSUMOTO M., IHIZAKI H., MATSUOKA C., ICHIKAWA, Y. & SHIMAHARA, A. 1988 Aerodynamic effects of the angle of attack upon a rectangular prism. *Journal of Wind Engineering and Industrial Aerodynamics* **77** & **78,** 531–542.

MATSUMOTO, M., YOKOYAMA, K., MIYATA, T., FUJINO, Y. & YAMAGUCHI, H. 1989 Wind induced cable vibration of cable-stayed bridges in Japan. *Proceedings of Japan-Canada Joint Workshop on Bridge Aerodynamics* pp. 101–110.

MATSUMOTO, M., ITO, Y., YAGI, T., TOKUMOTO, S., BAEK, B. & SHIRAISHI, N. 1991 On the enhancement properties of shear layer instability around bridge section by applied sound. Annals, Disaster Prevension Research Institute, Kyoto University, No.34, B-1, 57–69 (in Japanese)..

MATSUMOTO, M., SHIRAISHI, N. & SHIRATO, H. 1992 Rain–wind induced vibration of cables of cable-stayed bridges. *Journal of Wind Engineering and Industrial Aerodynamics* **41–44,** 2011–2022.

MATSUMOTO, M. 1998 Observed behavior of prototype cable vibration and its generation mechanism. *Proceedings of the International Symposium on Advances in Bridge Aerodynamics*, pp. 189–212.

MIZOTA, T. & OKAJIMA, A. 1981 Experimental studies of time mean flows around rectangular prisms. *Journal of the Japan Society of Civil Engineering*, 39–47 (in Japanese).

NAKAGAWA, K., KISHIDA, K. & IGARASHI, K., 1983 Aerodynamic vibration and wake characteristics of a yawed circular cylinder. Wind Tunnel Report of Osaka University 34–43 (in Japanese)

NAKAGUCHI, H., HASHIMOTO, K. & MUTO, M. 1968 An experimental study on aerodynamic drag of rectangular cylinders. *Journal of Japan Society of Aeronautical Engineering* **16,** 1–5 (in Japanese).

NAKAMURA, Y. & NAKASHIMA, M. 1986 Vortex excitation of prisms with elongated rectangular, H and ⊢ cross-sections. *Journal of Fluid Mechanics* **163,** 149–169.

PARKER, R. & WELSH, M. C. 1983 Effects of sound on flow separation of blunt flat plates. *International Journal of Heat & Fluid Flow* **4,** 113–127.

ROCKWELL, D. & KNISELY, C. 1978 The organized nature of flow impingement upon a corner. *Journal of Fluid Mechanics* **93,** 413–432.

SHIMADA, K. & MENG, Y. 1998 Numerical analysis for the aerodynamic statistics of rectangular cylinders and aeroelastic vibration of $B/D = 2$ rectangular cylinder by $k - \varepsilon$ model. *Proceedings of the 15th National Symposium on Wind Engineering*, pp. 161–166 (in Japanese).

SHIRAISHI, N. & MATSUMOTO, M. 1981 Vortex-induced oscillation of bluff bodies. *Proceedings of JSCE*, pp. 3–12 (in Japanese).

SHIRAISHI, N. & MATSUMOTO, M. 1983 On classification of vortex-induced oscillation and its application for bridge structures. *Journal of Wind Engineering and Industrial Aerodynamics* **15,** 419–430.

SHIRAISHI, N. & MATSUMOTO, M. 1984 On physical mechanism of vortex-induced oscillation and its response evaluation. *Journal of Wind Engineering, Japan Association for Wind Engineering*, 103–128 (in Japanese).

SHIRAKASHI, M., ISHIDA, Y. & WAKIYA, S. 1985 Higher velocity response of circular cylinders. *ASME journal of Fluids Engineering* **107,** 392–396.

WILLIAMSON, C. H. K. 1986 Oblique and parallel models of vortex-shedding in the wake of a circular cylinder at low Reynolds number. *Journal of Fluid and Mechanics* **206,** 579–627.